The Role of Photoisomerisation on the Photodetachment of the Photoactive Yellow Protein Chromophore

Alice Henley, Anand M. Patel, Michael A. Parkes, James C. Anderson, and Helen
H. Fielding*

Department of Chemistry, University College London, UK

E-mail: h.h.fielding@ucl.ac.uk

1

Abstract

The photocycle of photoactive yellow protein (PYP) is initiated by a photoinduced *trans-cis* isomerisation around a C=C bond in the chromophore that lies at the heart of the protein; however, in addition to the desired photochemical pathway, the chromophore can undergo competing electronic relaxation processes. Here, we combine gas-phase anion photoelectron spectroscopy and quantum chemistry calculations to investigate how locking the C=C bond in the chromophore controls the competition between these electronic relaxation processes following photoexcitation in the range 400-310 nm. We find evidence to suggest that preventing *trans-cis* isomerisation effectively turns off internal conversion to the ground electronic state and enhances electron emission from the first electronically excited state.

Introduction

Photoactive yellow protein (PYP) is a small protein responsible for the photophobic response of *Halorhodospira halophila* to potentially damaging UV light.[1] The chromophore of PYP, a deprotonated *para*-coumaric acid anion (pCA$^-$), is covalently bound to a cysteine residue and enclosed within the protein where it is stabilised by a network of hydrogen bonds. The first steps of the PYP photocycle occur following photoexcitation of the first excited singlet state of the chromophore ($\lambda_{\max} \sim 400$ nm) and involve a *trans-cis* isomerisation around the C=C bond in the chromophore followed by protonation of the chromophore. In the protein, isomerisation proceeds *via* a volume-conserving bicycle-pedal or hula-twist motion rather than a simple one-bond flip.[2] The small-scale motion of the chromophore in PYP induces large-scale conformational changes of the protein to form a long-lived signalling state; the photocycle then continues and eventually regenerates PYP in its initial state. However, in addition to the desired photochemical pathway, the chromophore that lies at the heart of PYP can undergo competing electronic relaxation processes such as internal conversion and electron emission.[3–7] The role played by the protein in controlling the competition between

2

these competing processes is a subject of ongoing discussion.

Gas-phase studies of isolated protein chromophores, free from interactions with protein or solvent environments, continue to play an important role in improving our understanding of the intrinsic electronic structure and relaxation dynamics of the chromophore. Studies of isolated PYP chromophores in the gas-phase have included analogues of pCA$^-$ and its methyl ester pCE$^-$, with variations in the ester tail of the chromophore,[6] with the hydroxyl motif in different positions on the phenol ring[5] and with different deprotonation sites.[8] Recent work in our group employed anion photoelectron spectroscopy and quantum chemistry calculations to investigate the competition between internal conversion and electron emission in model PYP chromophores with aliphatic bridges across the two single bonds either side of the C=C moiety.[7] We found that both of these single bond rotations assisted in efficient internal conversion from S_1 to S_0 but that torsional motion around the bond between the phenolate and C=C moieties was the most important. Phenolate-alkene single bond rotation was also found to play an important role in internal conversion from high-lying electronically excited states to the first excited state.

There have also been many studies of PYP and isolated PYP chromophores in solution aimed at understanding the role of torsional motions in the chromophore. These have included isolated chromophores with conformational locks around the single bonds either side of the unsaturated C=C bond at the centre of the chromophore[9] and around the C=C bond itself.[3,10,11] Hellingwerf and coworkers reconstructed PYP with non-isomerising analogues of pCA$^-$ in which the C=C bond was locked by bridging across it using an ester linkage (introducing an additional ester moeity) or by replacing the C=C bond by a C≡C bond.[11] It was found that both chromophores allowed access to the photocycle, which led to the suggestion that rotation about the C=C bond was not essential for PYP to function. Later work determined that the absorption for the ester-bridged chromophore was blue-shifted and the excited state lifetime was much longer (3 ns compared with 2 ps for the unlocked equivalent), suggesting that isomerisation around the double bond was essential for fast

internal conversion to the electronic ground state.[3] These studies have contributed significantly to our interpretation of the excited state dynamics of the PYP chromophore; however, the isomerisation-locked chromophores employed all had additional functionalities and it is possible that these may have obscured subtle differences in excited state behaviour, intrinsically or through interactions between the protein or solvent. Moreover, the importance of double-bond isomerisation on competing photoionisation processes is relatively unexplored.

In this paper, we report a combined anion photoelectron spectroscopy and computational chemistry study aimed at determining the role of torsional motions around the C=C bond on electron emission processes following photoexcitation of electronically excited states of PYP. We have designed and synthesised an analogue of the PYP chromophore with an ethane bridge inhibiting the double bond rotation, EBpCE$^-$ (Fig. 1). EBpCE$^-$ is a unique C=C photoisomerisation-locked PYP chromophore in which there are no additional functional groups and in which the strain introduced by the lock is minimised by employing a 6-membered ring. Although the single bond connecting the alkene to the ester moiety is also locked, we have already shown that rotation around this bond is not as important as rotation around the single bond connecting the alkene to the phenolate moiety.[7] We compare the electronic relaxation processes following photoexcitation of the locked chromophore, EBpCE$^-$, with a model PYP chromophore, pCE$^-$, which is the methyl ester of pCA$^-$.
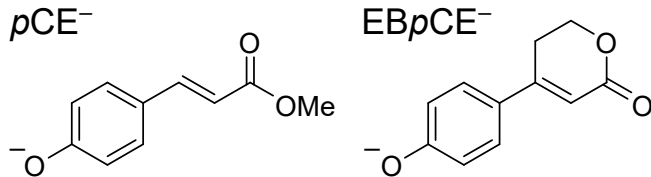

Figure 1: Structures of the chromophores used in this study: model PYP chromophore pCE$^-$ and the ethane-bridged chromophore EBpCE$^-$.

4

Experimental and computational methods

Chromophores

pCE was purchased from Tokyo Chemical Industry and used without further purification and EBpCE was prepared by methods described in detail in the supporting information.

Photoelectron spectroscopy

The anion photoelectron spectrometer combines electrospray ionisation (ESI) and a photo-electron velocity map imaging (VMI) setup and has been detailed elsewhere.[5–7,12–18] In brief, deprotonated anions were produced by electrospray ionisation (ESI) of a ~1 mM solution of pCE$^-$ or EBpCE$^-$ in methanol with a few drops of aqueous ammonia added. The isolated anions were mass-selected by a quadrupole and guided into a hexapole ion-trap from which they were released at a rate to match the repetition rate of the laser system. The anions coincided with pulses of laser light in the photodetachment region of a VMI photoelectron spectrometer. Nanosecond laser pulses of wavelength 310–346 nm were generated by frequency-doubling the output of a Nd:YAG pumped dye laser operating at 20 Hz and femtosecond pulses of wavelength centered at ~400 nm were produced by frequency-doubling the output of a commercial amplified Ti:Sapphire femtosecond laser system operating at 250 Hz. Photoelectrons generated in the photodetachment region were accelerated towards a position sensitive detector and imaged using a CCD camera. Laser-only images were recorded in the absence of the pulsed ion beam and subtracted from the overall signal to remove background counts. Photoelectron velocity distributions were obtained using the pBasex inversion method.[19] Electron kinetic energy (eKE) spectra were obtained by calibrating the radial photodetachment spectrum of iodide[20] (310–346 nm), deprotonated indole[21] (397.85 nm) and pHBDI$^-$ [15] (400 nm). The energy resolution of the 310–346 nm spectra is $\Delta E/E < 5\%$ and that of the ~400 nm spectra $\Delta E/E \approx 14\%$. The temporal window used to collect electrons was 75 ns, so these experiments measure only a fraction of electrons arising from thermionic emission,

which occurs on a millisecond timescale.

Calculations

The computational methods are described in full in Ref. 7. Briefly, the structures were optimised and vibrational analyses performed to confirm the structures were true minima at the B3LYP[22–25]/6-311++G(3df,3pd)[26–28] level of theory. Vertical excitation energies (VEEs) were calculated for the singlet states of the chromophores using both TD-CAMB3LYP[29]/6-311++G(3df,3pd) and ADC(2)[30,31]/6-31+G** methods. Vertical detachment energies (VDEs) were calculated using the electron propagator theory method,[32] EPT/6-311++G(3df,3pd), and the equation of motion coupled cluster with single and double excitations method for calculating ionisation potentials,[33] EOM-IP-CCSD/aug-cc-pVDZ.[34] The vertical and adiabatic detachment energies were also calculated as the anion-neutral energy difference, accounting for zero point energy, from B3LYP/6-311++G(3df,3pd) calculations. Canonical heat capacities were obtained from frequency calculations in order to estimate the temperature of the neutral radical following thermionic emission. Geometry optimisations, vibrational frequency, TD-DFT and EPT calculations were carried out using the Gaussian09 suite of programmes,[35] and the EOM-IP-CCSD and ADC(2) calculations were performed using Q-Chem.[36]

Results and discussion

Photoelectron spectra of EBpCE$^-$ are presented alongside those of the reference chromophore pCE$^-$, both as a function of electron kinetic energy (eKE) and electron binding energy ($eBE = h\nu - eKE$) in Fig. 2. Combs on the spectra plotted as a function of eBE mark calculated VDEs and VEEs. All the spectra have similar profiles: a broad feature at low eBE (high eKE, defined as $eKE > 0.2$) and a sharp feature at high eBE (low eKE, defined as $eKE < 0.2$). The features at low eBE have sharp rising edges that remain at constant

eBE with increasing photon energy, signifying that the low eBE peaks arise from direct photodetachment (PD) to the D_0 continuum, agreeing well with the calculated VDEs. These peaks broaden out towards higher eBE at higher photon energies, typical of the presence of an indirect process *via* a high-lying electronically excited state.
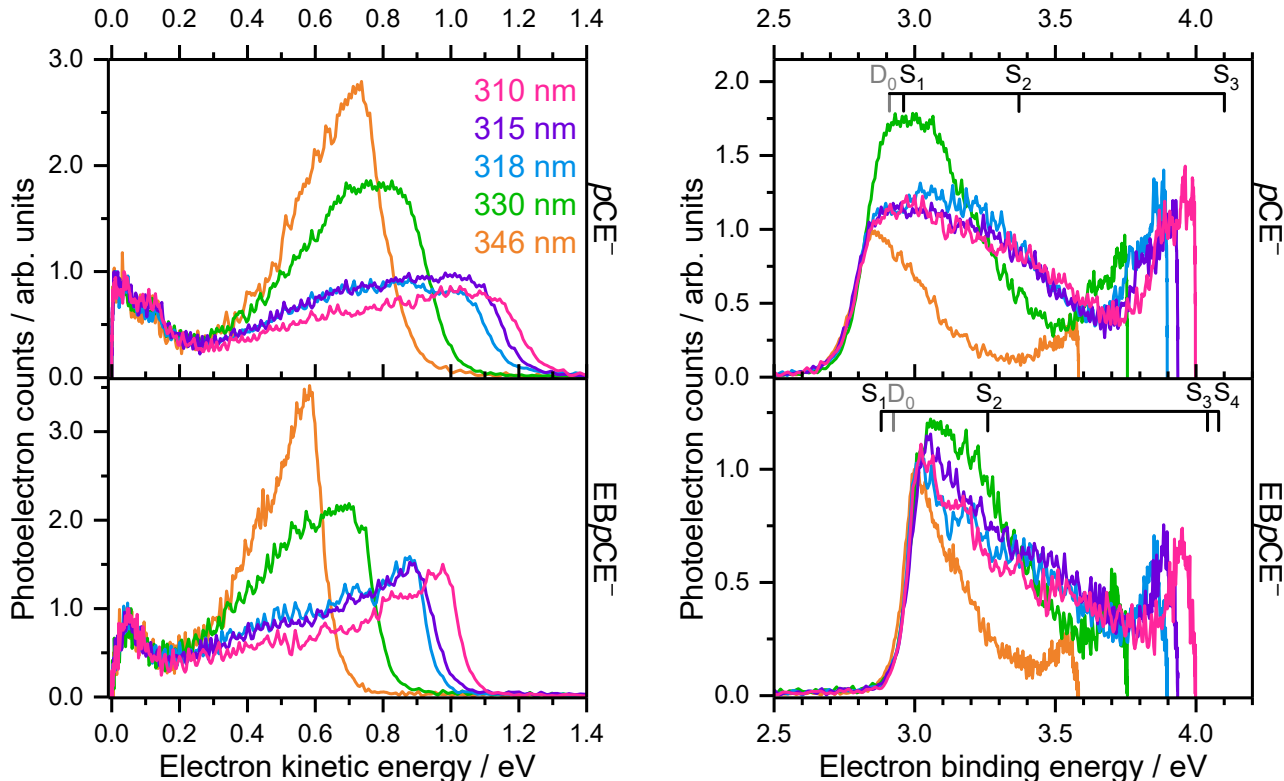

Figure 2: Photoelectron spectra presented as a function of electron kinetic energy, eKE, (left) and electron binding energy, eBE, (right) for the model PYP chromophore pCE$^-$ (top) and the isomerisation-locked chromophore EBpCE$^-$ (bottom). Spectra were recorded at 310 nm (4.00 eV), 315 nm (3.94 eV), 318 nm (3.90 eV), 330 nm (3.76 eV) and 346 nm (3.58 eV). Intensities of the eKE spectra are normalised to the maxima of the low eKE features (at eKE~0.06 eV) while the eBE spectra have been scaled to align the rising edges and are normalised to the maxima of the rising edges of the 346 nm spectra. Combs mark the EPT calculated VDEs (grey) and singlet excited states of the anion calculated using ADC(2)/6-31+G** (black).

The various PD pathways discussed in this work are illustrated in Figure 3 and include direct detachment, autodetachment following resonant excitation and thermionic emission (TE) from the hot ground electronic state. Electron emission from the ground-state or from low-lying excited states follows internal conversion (IC) from higher-lying excited states;

for example, autodetachment from the $1\pi\pi^*$ state could follow IC from $2\pi\pi^*$, similar to observations in model green fluorescent protein chromophores[12,14–16,37,38] and the luciferin chromophore.[18]
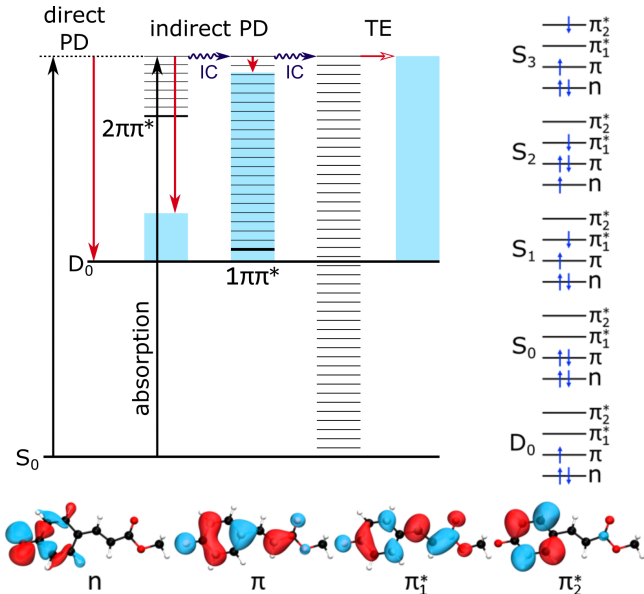

Figure 3: Jablonski diagram illustrating the major photodetachment (PD) pathways (red arrows) possible for $p\text{CE}^-$ and $\text{EB}p\text{CE}^-$ following UV absorption (346-310 nm). Pathways include internal conversion (IC) and thermionic emission (TE). Vibrational states of the electronic states of the anion are represented by horizontal black lines. Residual vibrational energy in the neutral radical following electron emission is represented by blue shaded boxes. Note that although the $1\pi\pi^*$ state is unbound in $p\text{CE}^-$, as represented in this Jablonski diagram, it is bound in $\text{EB}p\text{CE}^-$. Right: Electron configurations; S_1, S_2 and S_3 refer to the $1\pi\pi^*$, $1n\pi^*$ and $2\pi\pi^*$ excited states. Bottom: the main molecular orbitals involved in the first three singlet excited state of $p\text{CE}^-$ (see SI for orbitals of $\text{EB}p\text{CE}^-$).

It is clear from the spectra that the two chromophores have very similar detachment thresholds, although the VDE for $\text{EB}p\text{CE}^-$ is slightly higher than that for $p\text{CE}^-$. Table 1 lists experimental VDEs determined from the maxima of the 346 nm spectra, since this wavelength corresponds to a minimum in the absorption spectrum of $p\text{CE}^-$,[39] alongside VDEs and adiabatic detachment energies (ADEs) calculated using various computational methods. The DFT VDEs and ADEs of $\text{EB}p\text{CE}^-$ are close to one another, suggesting that the optimised geometries of the anion and the radical are similar, in agreement with earlier work on other model PYP chromophores.[5–7] The calculated VDEs are all within $\sim$0.1 eV

of the experimental maxima of the 346 nm spectra. The EPT method performed best, so it is the EPT values that are plotted in Fig. 2. The D_1 VDEs calculated with EPT and EOM-IP-CCSD are found to be significantly higher than the photon energies used in this work (≤ 4 eV) and thus it is unlikely that we observe electron detachment to higher lying $D_{n>0}$ continua.

Table 1: Detachment energies of EBpCE$^-$ calculated using EPT/6-311++G(3df,3pd), EOM-IP-CCSD/aug-cc-pVDZ and DFT/6-311++G(3df,3pd) given in eV. Pole strengths are shown in parentheses.

	pCE$^-$		EBpCE$^-$	
method	D_0	D_1	D_0	D_1
EPT	2.91 (0.879)	5.33 (0.873)	3.05 (0.987)	5.25 (0.874)
EOM-IP-CCSD	2.78	4.42	2.93	4.50
B3LYP VDE[a]	3.01		3.15	
B3LYP ADE (0-0)[a]	2.91		3.050	
Experiment[b]	2.85±0.05		3.02±0.05	

[a]Calculated as the D_0–S_0 energy difference, accounting for zero-point energies; [b]Maximum of the experimental 346 nm photoelectron spectrum.

Vertical excitation energies have been calculated using the ADC(2)/6-31+G** method and are presented in Table 2 for the excited singlet states of the anion accessible with the photon energies employed in this work. The ADC(2) method has been shown to be in excellent agreement with experiment[8] and high-level theory[40] for pCE$^-$ and other model PYP chromophores.[7] TD-CAM-B3LYP VEEs have also been calculated (also shown in Table 2). The first three singlet excited states of pCE$^-$ and EBpCE$^-$ were found by both methods to include $1\pi\pi^*$, $1n\pi^*$ and $2\pi\pi^*$ character as the main contributions and the respective electron configurations are shown in Fig. 3. It is worth noting that although we refer to the excited states by the character of their main component, the states involved in these ADC(2)-calculated transitions have significant configurational mixing (Table S1-2). Unlike the excited singlet states of pCE$^-$, for EBpCE$^-$ the $\pi_2^* \leftarrow \pi$ transition was found to be the main contribution in calculated transitions to both the S_3 and S_4 electronically excited states (Table 2). However, the ADC(2) VEEs and oscillator strengths for transitions to S_3 and S_4 are very close, suggesting that the two states are strongly coupled; therefore, these

transitions are discussed as the same transition ($2\pi\pi^* \leftarrow S_0$). Otherwise, the calculated electronic structures and orbitals of pCE$^-$ and EBpCE$^-$ are similar to each other (see Figure S5 for EBpCE$^-$ orbitals). Oscillator strengths for both chromophores have been calculated to be near unity for transitions to the $1\pi\pi^*$ states and zero (optically dark) for transitions to the $1n\pi^*$ states. The oscillator strengths for transitions to the $2\pi\pi^*$ states are low, yet significant, with those for EBpCE$^-$ being roughly half that for pCE$^-$. The π and π_1^* orbitals are delocalised across the whole anion, whereas the n and π_2^* orbitals are more localised towards the phenolate ends of the chromophores; thus, the transitions to the $1n\pi^*$ and $2\pi\pi^*$ states have significant charge transfer character. The electron configurations for the excited electronic states of the anions are also shown in Fig. 3 and are useful in determining the resonance character and providing a rough guide to autodetachment lifetimes of excited states lying in the D_0 continua. For example, electron detachment from $1\pi\pi^*$ or $2\pi\pi^*$ states to the D_0 continuum might be expected to be very fast as these states have shape and excited-shape resonance character with respect to D_0, respectively. Conversely, the $1n\pi^*$ state has Feshbach character with respect to the D_0 continuum and autodetachment from a Feshbach resonance is generally slower than from a shape resonance. Therefore, it is possible that if the Feshbach resonance is populated, there is time for $n\pi^* \to 1\pi\pi^*$ IC to occur. It is of course also possible that IC occurs directly from the higher lying $2\pi\pi^*$ state to $1\pi\pi^*$. It is worth noting that it is not only the resonance character of the excited electronic state that is important in defining the autodetachment lifetime but the vibrational modes that couple the electronically excited state with the continuum must also be considered.

Table 2: Calculated Vertical Excitation Energies at the TD-CAM-B3LYP and ADC(2) Levels of Theory (eV), oscillator strengths are shown in parentheses

		$1^1\pi\pi^*$ (S_1)	$1^1n\pi^*$ (S_2)	$2^1\pi\pi^*$ (S_3)	$2^1\pi\pi^*$ (S_4)
pCE$^-$	TD-CAM-B3LYP	3.43 (0.949)	4.12 (0.000)	4.31 (0.110)	-
	ADC(2)	2.96 (1.021)	3.37 (0.000)	4.10 (0.097)	-
EBpCE$^-$	TD-CAM-B3LYP	3.38 (0.765)	4.09 (0.001)	4.26 (0.024)	4.34 (0.090)
	ADC(2)	2.88 (0.871)	3.26 (0.000)	4.04 (0.024)	4.08 (0.025)

In the spectra in Figure 2, the low eBE peak broadens with increasing photon energy for both chromophores. Thus, locking the double-bond rotation appears to have little effect on autodetachment from the $2\pi\pi^*$ state. The eKE spectra for each chromophore have intensities in the low eKE region (0-0.4 eV) that are consistent in both shape and position for all wavelengths in the range 346–310 nm. In the case of pCE$^-$, the low eKE signal has a structured exponential profile and so we assign this to, predominantly, TE from vibrationally hot S_0, in agreement with earlier observations for pCE$^-$ and similar chromophores.[6,7] In contrast, the eKE spectra of EBpCE$^-$ have a low eKE peak that is much broader and does not have the distinct exponential profile characteristic of TE. Thus, it seems unlikely that this feature can be attributed to thermionic emission and we believe it is far more likely that it is the result of autodetachment from a low-lying electronically excited state (Fig. 3); this is discussed in more detail below when we describe the 400 nm photoelectron spectra. Comparing the intensities of the peaks in the photoelectron spectra, it can be seen that for both chromophores the low eKE (high eBE) peak has higher intensities relative to the high eKE (low eBE) peak at higher photon energies. This suggests that internal conversion to lower-lying electronic states becomes more important with increasing photon energy.

Fig. 4 shows the photoelectron spectra of pCE$^-$ and EBpCE$^-$ recorded following photoexcitation of the $1\pi\pi^*$ state at 400 nm (3.10 eV) overlaid on the 0-0.4 eV region of the spectra recorded at shorter wavelengths. The 400 nm spectra of both chromophores are dominated by features with approximately statistical profiles; however, they also have additional structure. At 400 nm, the VDEs of the two chromophores correspond to $eKE = h\nu - VDE = 0.25$ eV for pCE$^-$ and 0.10 eV for EBpCE$^-$. When the photon energy is very close to the detachment threshold, the cross-section for direct PD is expected to be relatively small and indeed the features observed at eKEs that correspond to VDEs are very small. The additional small feature in the photoelectron spectra of pCE$^-$ around 0.1 eV can be attributed to autodetachment from $1\pi\pi^*$; the propensity for conserving vibrational energy during photodetachment results in the emission of photoelectrons with $eKE = E(S_1) - VDE \approx 0.1$ eV. A similar fea-

ture has also been identified in photoelectron spectra of the pCA$^-$ model chromophore[7] (Fig. S2). These observations are consistent with earlier work from Zewail and coworkers in which it was found that 20% of the $1\pi\pi^*$ population of a keto analogue of the PYP chromophore underwent autodetachment.[41]
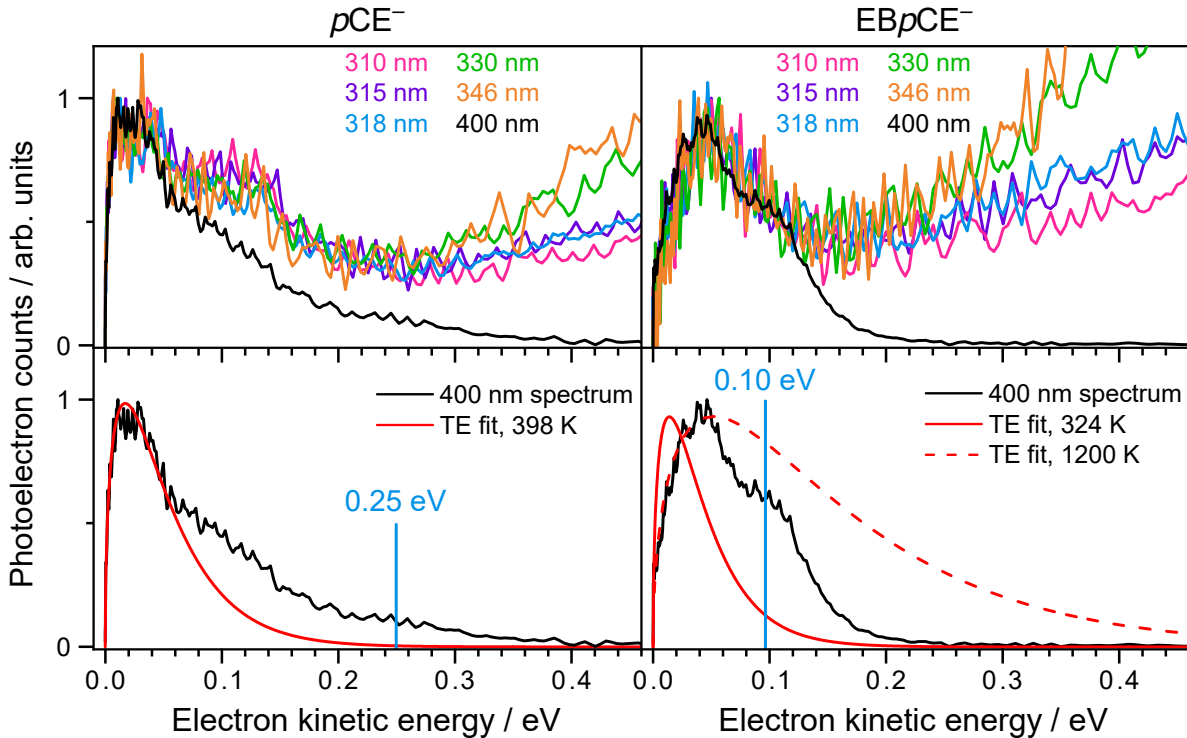

Figure 4: Photoelectron spectra presented as a function of electron kinetic energy, eKE for model PYP chromophore pCE$^-$ (left) and isomerisation-locked chromophore EBpCE$^-$ (right). Top panels show the $\sim$400 nm spectra overlaid on the spectra recorded with shorter wavelengths (346–310 nm) in the low eKE region. $\sim$400 nm spectra were recorded with λ_{max} as 400 nm (3.10 eV) for pCE$^-$ and 397.85 nm (3.12 eV) for EBpCE$^-$. Bottom panels show the 400 nm spectra with modelled thermionic emission curves using Klots' formula plotted at the temperatures specified. Intensities of the spectra are normalised to the maximum intensity and vertical blue lines mark the eKEs corresponding to the VDEs.

Although the 400 nm photoelectron spectra of both chromophores are dominated by features with approximately statistical profiles, they are strikingly different. For pCE$^-$, the overall profile is characteristic of thermionic emission from the ground state of the anion. The eKE distribution, $P(\epsilon)$, of electrons emitted by thermionic emission from anions has

been shown to be modelled well by Klots' formula,[42,43]

$$P(\epsilon) \propto \epsilon^{1/2} \exp(-\epsilon/k_B T_{M^\bullet}), \tag{1}$$

where k_B is Boltzmann's constant and $T_{M^\bullet}$ is the temperature of the resulting neutral radical,[44-46]

$$T_{M^\bullet} = T_{M^-} + (h\nu - \text{ADE})/C_v. \tag{2}$$

T_{M^-} is the initial temperature of the anions before photoexcitation and C_v is the microcanonical heat capacity. The microcanonical heat capacity $C_v \approx C_{\text{canonical}} - k_B \approx C_{\text{canonical}}$, since the heat capacities are $\sim 10^{-3}$ eV K^{-1}. Using estimations of $C_{\text{canonical}}$ from quantum chemistry calculations and assuming $T_{M^-} = 298$ K, $T_{M^\bullet}$ may be estimated as 398 K for $p\text{CE}^-$ and 324 K for EB$p\text{CE}^-$. Klots' formula (Eq. 1) fits the experimental data well for $p\text{CE}^-$ but does not fit the experimental data for the locked chromophore (Fig. 4). Attempting to fit just the rising edge of the 400 nm spectrum of EB$p\text{CE}^-$ requires an unreasonable value of $T_{M^\bullet} \approx 1200$ K. Thus, we conclude that $p\text{CE}^-$ undergoes internal conversion from the $1\pi\pi^*$ state to the ground state followed by thermionic emission, but that this is not possible for the locked chromophore; this is similar to our observations following photoexcitation at shorter wavelengths.

We attribute the dominant contribution to the 400 nm photoelectron spectrum of EB$p\text{CE}^-$ to autodetachment from the $1^1\pi\pi^*$ state that is directly excited at 400 nm. The approximately statistical profile suggests that the population is trapped in the S$_1$ state long enough to populate the vibrational modes that couple with the D$_0$ continuum. Similarly, following photoexcitation of the $2^1\pi\pi^*$ state at shorter wavelengths, it appears that population undergoes internal conversion to the $1^1\pi\pi^*$ state where it is then trapped whilst it undergoes vibrational redistribution and then autodetachment. At first sight, this may seem at odds with the fact that the vibrationally excited states of $1^1\pi\pi^*$ that lie above the adiabatic detachment limit have shape resonance character with respect to the D$_0$ continuum. However, it

13

can be explained by considering the propensity for conserving vibrational energy during photodetachment that results in the emission of photoelectrons with $eKE = E(S_1) - VDE$. For EBpCE$^-$, $E(S_1) < VDE$, which makes it impossible to conserve vibrational energy during the photodetachment process and suggests that the vibrational overlap between $1^1\pi\pi^*$ and D$_0$ will be small. This gives time for vibrational redistribution to populate the vibrational modes coupling the S$_1$ state to the D$_0$ continuum that are not populated directly at 400 nm, or indirectly following internal conversion from the $2^1\pi\pi^*$ state at shorter wavelengths. It would certainly be interesting to carry out high level quantum chemistry calculations to model the photoelectron spectra[38] and identify the coupling modes.

Overall, it appears that locking double bond rotation in the isolated PYP chromophore in the gas-phase effectively turns off ultrafast internal conversion to the ground state and traps population in the $1^1\pi\pi^*$ state. This is in line with observations of PYP chromophores in solution by Larsen *et al.* in which it was reported that locking the double-bond rotation increased the lifetime of the first excited state from 2 ps to 3 ns.[3] It is also in line with the theoretical predictions of Groenhof *et al.* who proposed that on the potential energy surface of the first excited state of the protein, the global minimum and conical intersection with the ground state both lie along the double bond rotation coordinate.[47,48]

The ability to turn off internal conversion to the ground electronic state and effectively trap population in the first electronically excited state is significant as it increases the probability for electron emission from the excited state. Electron emission has been observed from higher lying electronically excited states of the PYP chromophore that above the threshold for forming a solvated electron, both in aqueous solution[3] and in the protein.[4] Not only is the generation of solvated electrons very topical,[49-53] but the possibility of engineering proteins in which electron emission can occur from the first electronically excited state opens up the possibility of designing proteins with specific redox properties.[54,55]

14

Summary

In summary, we have employed a combination of anion photoelectron spectroscopy and quantum chemistry calculations to investigate the competition between electronic relaxation pathways in the model PYP chromophore pCE$^-$ and a non-isomerising analogue. We found that locking the double-bond rotation impedes internal conversion from the first electronically excited state to the ground state in the gas-phase, leaving electron detachment from the first electronically excited state as the main electronic relaxation pathway. These results suggest that a PYP analogue with an isomerisation-locked chromophore might have interesting light-induced redox properties, which opens up the exciting possibility of new device applications.

Acknowledgement

Supporting Information Available

Preparation and characterisation of EBpCE; photoelectron images; 400 nm spectra of pCA$^-$ and pCE$^-$; structural comparisons; vertical excitation energies and optimised geometries.

References

(1) Hellingwerf, K. J.; Hendriks, J.; Gensch, T. Photoactive Yellow Protein, A New Type of Photoreceptor Protein: Will This "Yellow Lab" Bring Us Where We Want to Go? *J.*

Phys. Chem. A **2003**, *107*, 1082–1094.

(2) Jung, Y. O.; Lee, J. H.; Kim, J.; Schmidt, M.; Moffat, K.; Šrajer, V.; Ihee, H. Volume-Conserving *trans-cis* Isomerization Pathways in Photoactive Yellow Protein Visualized by Picosecond X-Ray Crystallography. *Nat. Chem.* **2013**, *5*, 212–220.

(3) Larsen, D. S.; Vengris, M.; van Stokkum, I. H.; van der Horst, M. A.; de Weerd, F. L.; Hellingwerf, K. J.; van Grondelle, R. Photoisomerization and Photoionization of the Photoactive Yellow Protein Chromophore in Solution. *Biophys. J.* **2004**, *86*, 2538–2550.

(4) Zhu, J.; Paparelli, L.; Hospes, M.; Arents, J.; Kennis, J. T. M.; Van Stokkum, I. H. M.; Hellingwerf, K. J.; Groot, M. L. Photoionization and Electron Radical Recombination Dynamics in Photoactive Yellow Protein Investigated by Ultrafast Spectroscopy in the Visible and Near-Infrared Spectral Region. *J. Phys. Chem. B* **2013**, *117*, 11042–11048.

(5) Mooney, C. R. S.; Parkes, M. A.; Iskra, A.; Fielding, H. H. Controlling Radical Formation in the Photoactive Yellow Protein Chromophore. *Angew. Chem. Int. Ed.* **2015**, *54*, 5646–5649.

(6) Parkes, M. A.; Phillips, C.; Porter, M. J.; Fielding, H. H. Controlling Electron Emission from the Photoactive Yellow Protein Chromophore by Substitution at the Coumaric Acid Group. *Phys. Chem. Chem. Phys.* **2016**, *18*, 10329–10336.

(7) Henley, A.; Diveky, M. E.; Patel, A. M.; Parkes, M. A.; Anderson, J. C.; Fielding, H. H. Electronic Structure and Dynamics of Torsion-Locked Photoactive Yellow Protein Chromophores. *Phys. Chem. Chem. Phys.* **2017**, *19*, 31572–31580.

(8) Rocha-Rinza, T.; Christiansen, O.; Rajput, J.; Gopalan, A.; Rahbek, D. B.; Andersen, L. H.; Bochenkova, A. V.; Granovsky, A. A.; Bravaya, K. B.; Nemukhin, A. V. et al. Gas Phase Absorption Studies of Photoactive Yellow Protein Chromophore Derivatives. *J. Phys. Chem. A* **2009**, *113*, 9442–9449.

(9) Stahl, A. D.; Hospes, M.; Singhal, K.; van Stokkum, I.; van Grondelle, R.; Groot, M. L.; Hellingwerf, K. J. On the Involvement of Single-Bond Rotation in the Primary Photochemistry of Photoactive Yellow Protein. *Biophys. J.* **2011**, *101*, 1184–1192.

(10) Vengris, M.; van der Horst, M. A.; Zgrablić, G.; van Stokkum, I. H. M.; Haacke, S.; Chergui, M.; Hellingwerf, K. J.; van Grondelle, R.; Larsen, D. S. Contrasting the Excited-State Dynamics of the Photoactive Yellow Protein Chromophore: Protein versus Solvent Environments. *Biophys. J.* **2004**, *87*, 1848–1857.

(11) Cordfunke, R.; Kort, R.; Pierik, A.; Gobets, B.; Koomen, G.-J.; Verhoeven, J. W.; Hellingwerf, K. J. *Trans/cis* (*Z/E*) Photoisomerization of the Chromophore of Photoactive Yellow Protein is not a Prerequisite for the Initiation of the Photocycle of this Photoreceptor Protein. *Proc. Natl. Acad. Sci. U. S. A.* **1998**, *95*, 7396–7401.

(12) Mooney, C. R. S.; Parkes, M. A.; Zhang, L.; Hailes, H. C.; Simperler, A.; Bearpark, M. J.; Fielding, H. H. Competition between Photodetachment and Autodetachment of the $2^1\pi\pi^*$ State of the Green Fluorescent Protein Chromophore Anion. *J. Chem. Phys.* **2014**, *140*, 205103.

(13) Mckay, A. R.; Sanz, M. E.; Mooney, C. R. S.; Minns, R. S.; Gill, E. M.; Fielding, H. H. Development of a New Photoelectron Spectroscopy Instrument Combining an Electrospray Ion Source and Photoelectron Imaging. *Rev. Sci. Instrum.* **2010**, *81*, 123101.

(14) Mooney, C. R. S.; Sanz, M. E.; McKay, A. R.; Fitzmaurice, R. J.; Aliev, A. E.; Caddick, S.; Fielding, H. H. Photodetachment Spectra of Deprotonated Fluorescent Protein Chromophore Anions. *J. Phys. Chem. A* **2012**, *116*, 7943–7949.

(15) McLaughlin, C.; Assmann, M.; Parkes, M. A.; Woodhouse, J. L.; Lewin, R.; Hailes, H. C.; Worth, G. A.; Fielding, H. H. *Ortho* and *para* Chromophores of Green Fluorescent Protein: Controlling Electron Emission and Internal Conversion. *Chem. Sci.* **2017**, *8*, 1621–1630.

(16) Tay, J.; Parkes, M. A.; Addison, K.; Chan, Y.; Zhang, L.; Hailes, H. C.; Bulman Page, P. C.; Meech, S. R.; Blancafort, L.; Fielding, H. H. The Effect of Conjugation on the Competition between Internal Conversion and Electron Detachment: A Comparison between Green Fluorescent and Red Kaede Protein Chromophores. *J. Phys. Chem. Lett.* **2017**, *8*, 765–771.

(17) Beekmeyer, R.; Parkes, M. A.; Ridgwell, L.; Riley, J. W.; Chen, J.; Feringa, B. L.; Kerridge, A.; Fielding, H. H. Unravelling the Electronic Structure and Dynamics of an Isolated Molecular Rotary Motor in the Gas-Phase. *Chem. Sci.* **2017**, *8*, 6141–6148.

(18) Woodhouse, J. L.; Assmann, M.; Parkes, M. A.; Grounds, H.; Pacman, S. J.; Anderson, J. C.; Worth, G. A.; Fielding, H. H. Photoelectron Spectroscopy of Isolated Luciferin and Infraluciferin Anions *in vacuo*: Competing Photodetachment, Photofragmentation and Internal Conversion. *Phys. Chem. Chem. Phys.* **2017**, *19*, 22711–22720.

(19) Garcia, G. A.; Nahon, L.; Powis, I. Two-Dimensional Charged Particle Image Inversion Using a Polar Basis Function Expansion. *Rev. Sci. Instrum.* **2004**, *75*, 4989–4996.

(20) Arnold, D. W.; Bradforth, S. E.; Kim, E. H.; Neumark, D. M. Anion Photoelectron Spectroscopy of Iodine-Carbon Dioxide Clusters. *J. Chem. Phys.* **1992**, *97*, 9468–9471.

(21) Parkes, M. A.; Crellin, J.; Henley, A.; Fielding, H. H. A Photoelectron Imaging and Quantum Chemistry Study of the Deprotonated Indole Anion. *Phys. Chem. Chem. Phys.* **2018**, *20*, 15543–15549.

(22) Becke, A. D. Density-Functional Thermochemistry. III. The Role of Exact Exchange. *J. Chem. Phys.* **1993**, *98*, 5648–5652.

(23) Lee, C.; Yang, W.; Parr, R. G. Development of the Colle-Salvetti Correlation-Energy Formula into a Functional of the Electron Density. *Phys. Rev. B* **1988**, *37*, 785–789.

(24) Vosko, S. H.; Wilk, L.; Nusair, M. Accurate Spin-Dependent Electron Liquid Correlation Energies for Local Spin Density Calculations: A Critical Analysis. *Can. J. Phys.* **1980**, *58*, 1200–1211.

(25) Stephens, P. J.; Devlin, F. J.; Chabalowski, C. F.; Frisch, M. J. *Ab initio* Calculation of Vibrational Absorption and Circular Dichroism Spectra Using Density Functional Force Fields. *J. Phys. Chem.* **1994**, *98*, 11623–11627.

(26) Krishnan, R.; Binkley, J. S.; Seeger, R.; Pople, J. A. Self-Consistent Molecular Orbital Methods. XX. A Basis Set for Correlated Wave Functions. *J. Chem. Phys.* **1980**, *72*, 650–654.

(27) Clark, T.; Chandrasekhar, J.; Spitznagel, G. W.; Schleyer, P. V. R. Efficient Diffuse Function-Augmented Basis Sets for Anion Calculations. III. The 3-21+G Basis Set for First Row Elements, Li-F. *J. Comput. Chem.* **1983**, *4*, 294–301.

(28) Frisch, M. J.; Pople, J. A.; Binkley, J. S. Self-Consistent Molecular Orbital Methods 25. Supplementary Functions for Gaussian Basis Sets. *J. Chem. Phys.* **1984**, *80*, 3265–3269.

(29) Yanai, T.; Tew, D. P.; Handy, N. C. A New Hybrid Exchange-Correlation Functional Using the Coulomb-Attenuating Method (CAM-B3LYP). *Chem. Phys. Lett.* **2004**, *393*, 51–57.

(30) Schirmer, J. Beyond the Random-Phase Approximation: A New Approximation Scheme for the Polarization Propagator. *Phys. Rev. A* **1982**, *26*, 2395–2416.

(31) Trofimov, A. B.; Schirmer, J. An Efficient Polarization Propagator Approach to Valence Electron Excitation Spectra. *J. Phys. B: At., Mol. Opt. Phys.* **1995**, *28*, 2299–2324.

(32) Linderberg, J.; Öhrn, Y. *Propagators in Quantum Chemistry*; John Wiley and Sons: Hoboken, NJ, USA, 2014.

(33) Krylov, A. I. Equation-of-Motion Coupled-Cluster Methods for Open-Shell and Elec-
tronically Excited Species: The Hitchhiker's Guide to Fock Space. *Annu. Rev. Phys.
Chem.* **2008**, *59*, 433–462.

(34) Kendall, R. A.; Dunning Jr, T. H.; Harrison, R. J. Electron Affinities of the First-Row
Atoms Revisited. Systematic Basis Sets and Wave Functions. *J. Chem. Phys.* **1992**,
96, 6796–6806.

(35) Frisch, M. J.; Trucks, G. W.; Schlegel, H. B.; Scuseria, G. E.; Robb, M. A.; Cheese-
man, J. R.; Scalmani, G.; Barone, V.; Mennucci, B.; Petersson, G. A. et al. Gaussian
09, Revision D.01. 2009.

(36) Shao, Y.; Gan, Z.; Epifanovsky, E.; Gilbert, A. T. B.; Wormit, M.; Kussmann, J.;
Lange, A. W.; Behn, A.; Deng, J.; Feng, X. et al. Advances in Molecular Quantum
Chemistry Contained in the Q-Chem 4 Program Package. *Mol. Phys.* **2015**, *113*, 184–
215.

(37) West, C. W.; Bull, J. N.; Hudson, A. S.; Cobb, S. L.; Verlet, J. R. R. Excited State
Dynamics of the Isolated Green Fluorescent Protein Chromophore Anion Following UV
Excitation. *J. Phys. Chem. B* **2015**, *119*, 3982–3987.

(38) Bochenkova, A. V.; Mooney, C.; Parkes, M. A.; Woodhouse, J.; Zhang, L.; Lewin, R.;
Ward, J. M.; Hailes, H.; Andersen, L. H.; Fielding, H. Mechanism of Resonant Electron
Emission from the Deprotonated GFP Chromophore and its Biomimetics. *Chem. Sci.*
2017, 3154–3163.

(39) Rocha-Rinza, T.; Christiansen, O.; Rahbek, D. B.; Klærke, B.; Andersen, L. H.;
Lincke, K.; Brøndsted Nielsen, M. Spectroscopic Implications of the Electron Donor-
Acceptor Effect in the Photoactive Yellow Protein Chromophore. *Chem. Eur. J.* **2010**,
16, 11977–11984.

(40) Fernández García-Prieto, F.; Aguilar, M. A.; Fdez. Galván, I.; Muñoz-Losa, A.; Olivares del Valle, F. J.; Sánchez, M. L.; Martín, M. E. Substituent and Solvent Effects on the UV-Vis Absorption Spectrum of the Photoactive Yellow Protein Chromophore. *J. Phys. Chem. A* **2015**, *119*, 5504–5514.

(41) Lee, I.-R.; Lee, W.; Zewail, A. H. Primary Steps of the Photoactive Yellow Protein: Isolated Chromophore Dynamics and Protein Directed Function. *Proc. Natl. Acad. Sci. U. S. A.* **2006**, *103*, 258–262.

(42) Klots, C. E. Unimolecular Decomposition in a Spherically Symmetric Potential. *J. Chem. Phys.* **1993**, *98*, 1110–1115.

(43) Klots, C. E. Unimolecular Reactions in a Spherically Symmetric Potential. II. Some Tractable Potentials. *J. Chem. Phys.* **1994**, *100*, 1035–1039.

(44) Mabbs, R.; Surber, E.; Sanov, A. Photoelectron Imaging of Negative Ions: Atomic Anions to Molecular Clusters. *Analyst* **2003**, *128*, 765–772.

(45) Wills, J. B.; Pagliarulo, F.; Baguenard, B.; Lépine, F.; Bordas, C. Time and Kinetic Energy Resolved Delayed Electron Emission in Small Carbon Cluster Anions. *Chem. Phys. Lett.* **2004**, *390*, 145–150.

(46) Climen, B.; Pagliarulo, F.; Ollagnier, A.; Baguenard, B.; Concina, B.; Lebeault, M. A.; Lépine, F.; Bordas, C. Threshold Laws in Delayed Emission: An Experimental Approach. *Eur. Phys. J. D* **2007**, *43*, 85–89.

(47) Groenhof, G.; Bouxin-Cademartory, M.; Hess, B.; de Visser, S. P.; Berendsen, H. J. C.; Olivucci, M.; Mark, A. E.; Robb, M. A. Photoactivation of the Photoactive Yellow Protein: Why Photon Absorption Triggers a *trans*-to-*cis* Isomerization of the Chromophore in the Protein. *J. Am. Chem. Soc.* **2004**, *126*, 4228–4233.

(48) Groenhof, G.; Schäfer, L. V.; Boggio-Pasqua, M.; Grubmüller, H.; Robb, M. A. Arginine52 Controls the Photoisomerization Process in Photoactive Yellow Protein. *J. Am. Chem. Soc.* **2008**, *130*, 3250–3251.

(49) Elkins, M. H.; Williams, H. L.; Shreve, A. T.; Neumark, D. M. Relaxation Mechanism of the Hydrated Electron. *Science (80-.).* **2013**, *342*, 1496–1499.

(50) Abel, B. Hydrated Interfacial Ions and Electrons. *Annu. Rev. Phys. Chem.* **2013**, *64*, 533–552.

(51) Seidel, R.; Winter, B.; Bradforth, S. E. Valence Electronic Structure of Aqueous Solutions: Insights from Photoelectron Spectroscopy. *Annu. Rev. Phys. Chem.* **2016**, *67*, 283–305.

(52) Luckhaus, D.; Yamamoto, Y.-i.; Suzuki, T.; Signorell, R. Genuine Binding Energy of the Hydrated Electron. *Sci. Adv.* **2017**, *3*, e1603224.

(53) Riley, J. W.; Wang, B.; Woodhouse, J. L.; Assmann, M.; Worth, G. A.; Fielding, H. H. Unravelling the Role of an Aqueous Environment on the Electronic Structure and Ionization of Phenol Using Photoelectron Spectroscopy. *J. Phys. Chem. Lett.* **2018**, *9*, 678–682.

(54) Bogdanov, A. M.; Mishin, A. S.; Yampolsky, I. V.; Belousov, V. V.; Chudakov, D. M.; Subach, F. V.; Verkhusha, V. V.; Lukyanov, S.; Lukyanov, K. A. Green Fluorescent Proteins are Light-Induced Electron Donors. *Nat. Chem. Biol.* **2009**, *5*, 459–61.

(55) Acharya, A.; Bogdanov, A. M.; Grigorenko, B. L.; Bravaya, K. B.; Nemukhin, A. V.; Lukyanov, K. A.; Krylov, A. I. Photoinduced Chemistry in Fluorescent Proteins: Curse or Blessing? *Chem. Rev.* **2017**, *117*, 758–795.

Graphical TOC Entry